Available online at www.sciencedirect.com
SCIENCE DIRECT®
International Journal of Thermal Sciences 45 (2006) 443–451
International Journal of Thermal Sciences
www.elsevier.com/locate/ijts

# Thermal diffusivity measurements on a single fiber with microscale diameter at very high temperature

C. Pradère [a,b], J.M. Goyhénèche [b,*], J.C. Batsale [a], S. Dilhaire [c], R. Pailler [b]

[a] *TREFLE, UMR 8508, Esplanade des Arts et Métiers, 33405 Talence, France*
[b] *LCTS, UMR 5801, 3 allée de La Boétie, 33600 Pessac, France*
[c] *CPMOH, UMR 5798, 351 cours de la Libération, 33405 Talence, France*

Received 20 December 2004; received in revised form 7 April 2005; accepted 25 May 2005

Available online 27 January 2006

**Abstract**

The objective of this work is to measure the thermal diffusivity of single carbon and ceramic fibers at very high temperature. The difficulty of the measurement is due to the micrometric scale of the fiber (≈10 μm) and the important range of temperature (700–2700 K). An original periodic technique is developed. Based on a 1D analytical direct models and using both magnitude and phase shift measurements, it allows accurate results from simulated experiments. A device is designed in order to maintain the fiber at uniform high temperature. A small perturbation is imposed by a laser beam and the temperature response is analysed. A complete study of the numerical identification allows an estimation of the uncertainty due to the numerical process. For $a \pm \sigma$ standard deviation on experimental measurements, the thermal diffusivity is estimated with $a \pm \sigma/80$ uncertainty. Measurements on both low and high conductive materials validate the apparatus and the estimation method.


*Keywords:* Data processing method; Thermal diffusivity; Very high temperature and photothermal measurement

## 1. Introduction

Composite materials elaborated from carbon and/or ceramic components have very efficient properties at high temperature [1]: wide range of Young modulus, thermal conductivity, and coefficient of thermal expansion. These properties are especially attractive for applications in:

(i) aeronautics: carbon/carbon composites for brakes, ceramic matrix composites for engines;
(ii) aerospace: carbon/carbon composites for heat shields; and
(iii) nuclear reactors: carbon/carbon composites for control systems, SiC/SiC composites for combustible holder.

Further, the design of composites with a numerical approach needs a prior knowledge of the physical (thermal and mechanical) properties of each constituent, fiber and matrix, from room temperature to several thousands Kelvin. As a consequence, this work deals with the thermal diffusivity of fibers at very high temperature.

This property can be measured either on single filaments, on bundles (tow made with several thousands filaments embedded in a matrix), or finally on unidirectional composites [2]. In the two last cases, the estimation of the researched property needs the use of a constitutive model in order to deduce the thermal diffusivity of the fiber from the thermal diffusivity of the bundle or the composite, knowing the thermophysical properties (density, diffusivity, specific heat) and the geometric characteristics (volumetric fraction, morphology ...) of the other components (matrix, porosity). Another difficulty is to simply realise a bundle or a composite which can be used for experiments up to 2700 K. For these two reasons, the measurement developed in this work concerns single filaments.

## 2. Measurement method

Several kinds of experimental techniques have been developed to perform the thermal diffusivity of single filaments. At

* Corresponding author.
*E-mail address:* jean-marc.goyheneche@cea.fr (J.M. Goyhénèche).

1290-0729/$ – see front matter 
doi:10.1016/j.ijthermalsci.2005.05.010

**Nomenclature**

| | | |
|---|---|---|
| $c_p$ | specific heat | $\mathrm{J\,kg^{-1}\,K^{-1}}$ |
| $\boldsymbol{cov}$ | covariance matrix | |
| $d$ | fiber diameter | m |
| $f$ | frequency | Hz |
| $h$ | linearised heat losses coefficient | $\mathrm{W\,m^{-2}\,K^{-1}}$ |
| $k$ | thermal conductivity | $\mathrm{W\,m^{-1}\,K^{-1}}$ |
| $L$ | detection length of the infrared sensor | m |
| $N$ | number of measurements | |
| $p$ | perimeter of the wire | m |
| $\dot{q}$ | heat flux | $\mathrm{W\,m^{-2}}$ |
| $S$ | cross-section of the fiber | $\mathrm{m^2}$ |
| $S_{f,p}$ | sensitivity of the function f on the parameter $p$ | |
| $t$ | time | s |
| $T$ | temperature | K |
| $\widetilde{T}$ | periodic component of the fiber temperature | K |
| $z, \hat{z}$ | position along the wire | m |

*Greek symbols*

| | | |
|---|---|---|
| $\alpha$ | longitudinal thermal diffusivity | $\mathrm{m^2\,s^{-1}}$ |
| $\Delta\bullet$ | magnitude | |
| $\phi, \hat{\phi}$ | phase shift of the fiber periodic temperature | rad |
| $\omega$ | pulsation | $\mathrm{rad\,s^{-1}}$ |
| $\sigma$ | standard deviation | |
| $\sigma_B$ | Stefan–Boltzmann constant | $\mathrm{W\,m^{-2}\,K^{-4}}$ |
| $\rho$ | density | $\mathrm{kg\,m^{-3}}$ |

*Subscripts*

| | |
|---|---|
| $o$ | initial |
| $a$ | average |
| $i$ | relative to the imaginary part of $\gamma$ |
| $j$ | number of the experiment |
| $r$ | relative to the real part of $\gamma$ |
| $s$ | imposed on the fictive surface located at $z = a$ |
| rt | room temperature |

*Superscripts*

| | |
|---|---|
| $l$ | left side of the excitation |
| $m$ | measured |
| $r$ | right side of the excitation |

very low temperature (5 K to 300 K), L. Piraux et al. [3] and Issi et al. [4] have used a contact method. In their experiment, the temperature of the sample is measured by two thermocouples while the heat flux through the fiber is imposed by Joule effect. Then, the thermal conductivity is simply calculated by the Fourier law taking into account the heat losses along the sample. More recently, an equivalent method is proposed by Zhang et al. [5] for measurements at room temperature. In all these experiments in steady state, the measurement becomes very difficult when the heat losses at the surface of the fiber are important. It could be penalising at very high temperature.

This drawback is avoided using modulated methods. Kawabata [6] and more recently Yamane et al. [7] have used a periodic excitation from an halogen lamp, and a contact detection by thermocouple. The lamp is moved at different positions along the fiber. This experiment is realised from 300 K to 800 K, with a low frequency irradiation ($f < 1$ Hz), on a commercial apparatus (Sinku-Riko Inc., model PIT-1) described by Hatta et al. [8]. The sensor (Chromel–Alumel, diameter 12.5 μm) is directly stuck on the fiber (diameter ≈10 μm) with silver lacquer. The thermal diffusivity is calculated with a 1D non-adiabatic model, from the magnitude temperature response of the sample.

Another kind of method is based on a non-contact response detection. In this case, the excitation is generally realised by a laser beam. The mirage method, developed for the thermal characterisation by Barkoumb et al. [9] and Sanchez-Lavega et al. [10], is very difficult to apply on a single fiber. The detection is realised by the measurement of a laser beam deflection which is supposed linearly dependent of the temperature. Then, the identification of the thermal diffusivity is made by a 2D non-adiabatic model. Easier to realise, the photoreflective experiment uses the reflection of a second laser beam focalised near the excitation to measure a signal proportional to the temperature response of the sample. This method has been developed for the thermal characterisation of fibers by Jumel et al. [11] and Le Houdec et al. [12]. The experiment being made at very high frequency, the thermal diffusivity is identified with an adiabatic model. Finally, the detection of the thermal sample response can be made using the emission of the fiber, directly detected by an infrared sensor. Recently, Oksanen et al. [13] and Bisson et al. [14] have proposed photothermal microscopes using the phase shift between the irradiating laser beam and the detected emission in order to determine the thermal diffusivity of fibers.

In comparison with the previous studies, the very high temperature (700–2700 K) is the main constraint in this work. As a consequence (Fig. 1): (i) the filament will be warmed up by Joule effect, (ii) the steady state method, limited by the radiative heat losses at very high temperature, must be replaced by a periodic excitation, and (iii) the contact detection of the temperature must be replaced by an optical (infrared) sensor. Finally, because of the very small diameter of the fiber (≈10 μm), the periodic thermal excitation will be delivered by a laser beam focalised at the surface of the sample.

## 3. Experimental device

The experimental device is presented in Fig. 2. The fiber, stuck by its ends on two carbon grips, and warmed up by Joule effect (electric supply 0–50 mA, 0–300 V), is maintained at very low pressure ($<10^{-4}$ Pa) in a silica glass enclosure (≈25 mm diameter, ≈150 mm length) which allows the transmission of 90% emitting radiative flux from the sample to the detector. The position of the sample is adjusted using micrometer moving systems located into the enclosure and controlled

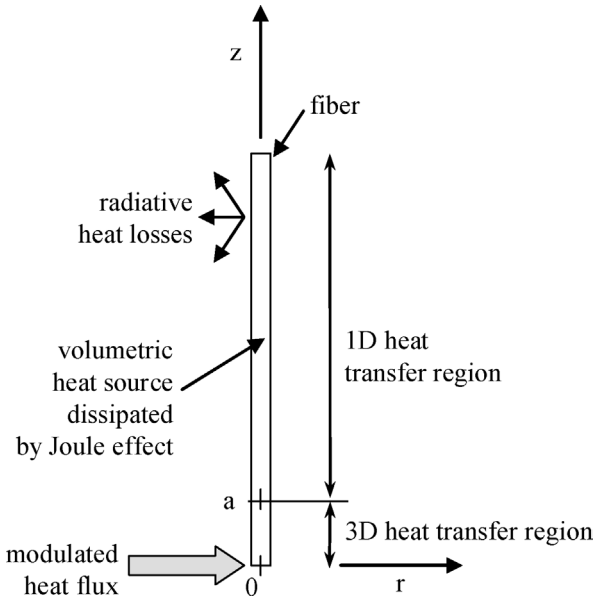


Fig. 1. Principle of the experiment.

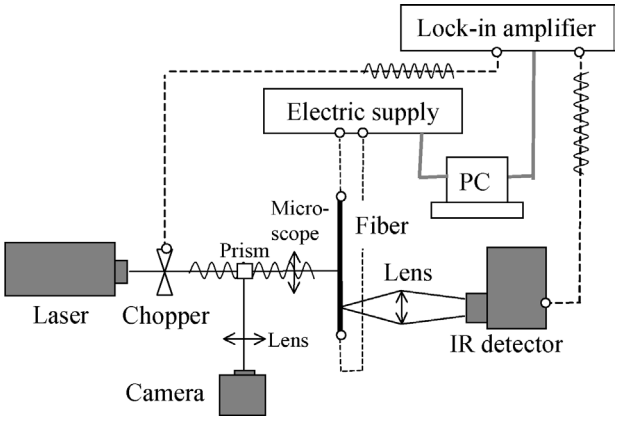


Fig. 2. Experimental device.

from the outside. A two colours pyrometer (IRCON special model, 0.75–1.05 μm, 3% uncertainty) measures the absolute temperature of the fiber over a detection zone of 300 μm diameter calculated via geometrical optics formulae. For a 10 micrometers fiber, the emissive area represents 4% of the pyrometer detection zone. This rate, greater than 1%, is sufficient to realise the measurement without size effect.

The thermal excitation is imposed by a modulated multimode Argon laser beam (power up to 200 mW, frequency from 0.1 to 50 Hz) focalised by a microscope objective (magnitude ×50, working distance 16 mm) on an irradiated zone of ≈ 2 μm diameter. This spot is evaluated from geometrical optics formulae, has been experimentally verified [15], and is controlled during the experiment with a CCD camera. This later is focalised on the fiber via a system composed by a lens (50 mm focus length), a splitting prism, and the objective. An infrared detector (PbSn, 1–3 μm, 1 $mm^2$ sensitive area, liquid $N_2$ cooled) associated with two plano-convex $BaCF_2$ lens (25 mm and 200 mm focus length) is used for the temperature response measurement, along the fiber (motorised displacement), over a detection zone of ≈125 μm diameter. This spot, equivalent to a detection length $L$ along the fiber, is evaluated from geometrical optics formulae, and systematically measured at the beginning of each experiment using a lateral scanning of fiber by the detector.

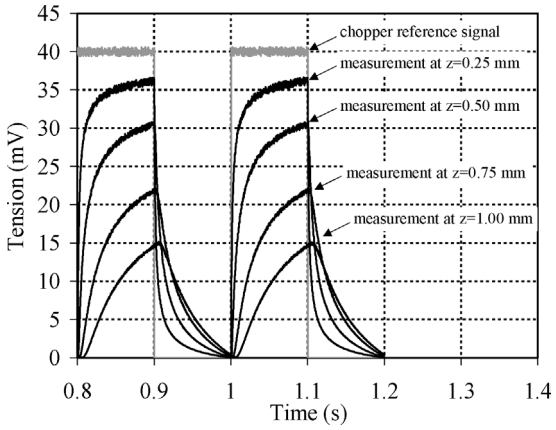


Fig. 3. Excitation and response measured signals on a P100 carbon fiber at $T_o = 1500$ K, $f = 5$ Hz.

During the experiment, a lock-in amplifier determines the magnitude and the phase shift between the electromechanical chopper and the temperature response detected by the infrared sensor. These measurements are transferred to a computer for several frequencies and positions of the infrared detector. Then, a data processing routine yields the slopes of the linear parts automatically detected on the records. This operation is realised from a local derivation of the experimental curves, following by a numerical filter.

An example of the experimental signals measured on a P100 carbon fiber (≈10 μm diameter, ≈50 mm length, $L \approx 150$ μm) at $T_o = 1500$ K, for several positions of the infrared detector, is presented (Fig. 3). A good ratio signal/noise (better than 500) on both excitation and response records is obtain, the radiative flux emitted by the background being very small compared to the fiber one. In addition, only the modulated part (not perturbated by the background radiation) of the detected signal is used to estimate the thermal diffusivity. As a consequence, the experimental signals yield a low uncertainty on the measured values.

## 4. 1D direct model for the fiber modulated temperature

The thermal problem, limited on the half of the fiber, is described in Fig. 1. The laser beam irradiates the sample at $z = 0$, corresponding to the middle of the fiber. From this abscissa to $z = a$, the temperature field is 3D. The distance $a$ depends on the fiber diameter and thermal properties. For $z > a$, the medium is supposed thermally thin and the temperature only depends on $z$: the temperature field becomes 1D. This assumption is validated by the calculation of an upper value for the Biot number: $Bi = h_o(d/2)/k_T$ where $h_o \approx 4\varepsilon\sigma_B T_o^3$ represents the radiative heat losses coefficient, $d$ the fiber diameter and $k_T$ its transverse thermal conductivity. For $\varepsilon = 1$, $T_o = 2700$ K, $d = 10$ μm and $k_T = 1\ \mathrm{W\,m^{-1}\,K^{-1}}$, one obtains $Bi = 0.02$ which is very small compared to 1.

In the case of an adiabatic anisotropic sample, the distance $a$ satisfies the relation: $a \gg \sqrt{(d^2/4)(\alpha_L/\alpha_T)}$ where $\alpha_L$ and $\alpha_T$ respectively represent the longitudinal and the transverse thermal diffusivity of the fiber. Typically, for metallic or ceramic fibers: $\alpha_L \approx \alpha_T$, and for carbon fibers: $\alpha_L/\alpha_T < 10$. Considering a 10 μm sample, $a$ must be widely greater than 15 μm. For high temperature experiment, the radiative losses tend to decrease this value. In practical, $a < 200$ μm in our experiments.

The measurement will be performed in the 1D region ($z > a$) where the temperature profile can be analytically calculated. So, in the following, the thermal problem will be limited by a fictive boundary at $z = a$ where a uniform temperature or heat flux modulated condition will be imposed. In order to facilitate the understanding, a new longitudinal abscissa is used in the analytical study: $\hat{z} = z - a$.

Moreover, the phase reference $\phi = 0$ is given by the excitation laser beam, at $z = 0$. At $z = a$, a phase shift $\phi_o$ exists between the temperature of the sample and the excitation laser beam. This is induced by the 3D heat transfer region. In order to facilitate the calculation, the phase reference is taken at $\hat{z} = 0$ (or $z = a$): $\hat{\phi} = \phi - \phi_o$.

With these assumptions, the analytical formulation of the thermal problem is written for $\hat{z} \geqslant 0$:

$$\begin{cases} k\frac{\partial^2 T(\hat{z},t)}{\partial \hat{z}^2} - \frac{h_o p(T(\hat{z},t)-T_{rt})}{S} = \rho c_p \frac{\partial T(\hat{z},t)}{\partial t} \\ \hat{z} = 0, \quad -k\frac{\partial T(\hat{z},t)}{\partial \hat{z}}\big|_0 = \dot{q}_s + \Delta\dot{q}_s \sin(\omega t) \\ \quad \text{or} \quad T(0,t) = T_s + \Delta T_s \sin(\omega t) \\ \hat{z} \to \infty, \quad T(\hat{z},t) \to T_o \\ T(\hat{z},0) = T_o \end{cases} \tag{1}$$

The amplitude of the temperature modulation (measured by the pyrometer) is ranging from several degrees at $T_o = 700$ K and several tens of degrees at $T_o = 2700$ K. It provides a relative temperature variation always lower than 3%, and a relative variation of the radiative heat transfer coefficient $h_o$, proportional to $T_o^3$, lower than 9% [16]. So, the heat losses coefficient $h_o$ is supposed constant in time and close to its value calculated at the temperature $T_o$:

$$h_o \approx 4\varepsilon\sigma_B T_o^3 \tag{2}$$

In order to obtain an analytical solution of this problem in a periodic established state, the temperature $T$ is separated in both average $T_a(\hat{z})$ and periodic $\widetilde{T}(\hat{z},t)$ components: $T(\hat{z},t) = T_a(\hat{z}) + \widetilde{T}(\hat{z},t)$. As a consequence, the system (1) yields:

$$\begin{cases} \frac{\mathrm{d}^2 T_a(\hat{z})}{\mathrm{d}\hat{z}^2} - \frac{h_o p(T_a(\hat{z})-T_{rt})}{kS} = 0 \\ \hat{z} = 0\text{: } -k\frac{\mathrm{d}T_a(\hat{z})}{\mathrm{d}\hat{z}}\big|_0 = \dot{q}_s \quad \text{or} \quad T_a(\hat{z}) = T_s \\ \hat{z} \to \infty\text{: } T_a(\hat{z}) \to T_o \end{cases} \tag{3}$$

for the average component and:

$$\begin{cases} k\frac{\partial^2 \widetilde{T}(\hat{z},t)}{\partial \hat{z}^2} - \frac{h_o p\widetilde{T}(\hat{z},t)}{S} = \rho c_p \frac{\partial \widetilde{T}(\hat{z},t)}{\partial t} \\ \hat{z} = 0\text{: } -k\frac{\partial \widetilde{T}(\hat{z},t)}{\partial \hat{z}}\big|_0 = \Delta\dot{q}_s \sin(\omega t) \\ \quad \text{or} \quad \widetilde{T}(\hat{z},t) = \Delta T_s \sin(\omega t) \\ \hat{z} \to \infty\text{: } \widetilde{T}(\hat{z},t) \to 0 \end{cases} \tag{4}$$

for the modulated component. The solution of (4) is obtained analytically for the temperature condition:

$$\widetilde{T}(\hat{z},t) = \left(\Delta T_s e^{-\gamma\hat{z}}\right)e^{i\omega t} \tag{5}$$

and for the heat flux condition:

$$\widetilde{T}(\hat{z},t) = \left(\frac{\Delta\dot{q}_s}{\gamma k}e^{-\gamma\hat{z}}\right)e^{i\omega t} \tag{6}$$

where $\gamma = \sqrt{\frac{h_o p}{kS} + i\frac{\omega}{a}} = \gamma_r + i\gamma_i$ with:

$$\gamma_r(\alpha, Q, f) = \frac{1}{\sqrt{\alpha}}\sqrt{Q + \sqrt{(Q)^2 + (\pi f)^2}}$$

$$\gamma_i(\alpha, Q, f) = \frac{1}{\sqrt{\alpha}}\sqrt{-Q + \sqrt{(Q)^2 + (\pi f)^2}}$$

$$Q = \frac{h_o p}{2\rho c_p S} \tag{7}$$

In these relations, $\alpha = k/\rho c_p$ ($\mathrm{m^2\,s^{-1}}$) represents the longitudinal thermal diffusivity of the sample and $f = \omega/2\pi$ (Hz) the frequency. The magnitude $\Delta\widetilde{T}$ and the phase shift $\hat{\phi}$ of the temperature modulation:

$$\widetilde{T} = \Delta\widetilde{T}\sin(\omega t + \hat{\phi}) \tag{8}$$

are then obtained from the relation (5) for the temperature condition:

$$\log\left[\Delta\widetilde{T}(\alpha, Q, f, \hat{z})\right] = -\gamma_r\hat{z} + \log[\Delta T_s] \tag{9}$$

$$\hat{\phi}(\alpha, Q, f, \hat{z}) = -\gamma_i\hat{z} \tag{10}$$

and from the relation (6) for the heat flux condition:

$$\log\left[\Delta\widetilde{T}(\alpha, Q, f, \hat{z})\right] = -\gamma_r\hat{z} + \log\left[\frac{\Delta\dot{q}_s}{k\sqrt{\gamma_r^2 + \gamma_i^2}}\right] \tag{11}$$

$$\hat{\phi}(\alpha, Q, f, \hat{z}) = -\gamma_i\hat{z} - \arctan\left[\frac{\gamma_i}{\gamma_r}\right] \tag{12}$$

In practical, the temperature detection along the fiber is realised with an infrared sensor which measures a modulated signal integrated over a length $L$ (≈125 μm) of the sample. Even if $L$ is smaller than the modulation attenuation length (i.e. the distance over which the signal cannot be detected, experimentally evaluated, and always greater than 1 mm), the temperature detected depends on it. As a consequence, the direct model must take into account this parameter. So, integrating the modulated component of the temperature (8) from $\hat{z}$ to $\hat{z} + L$, the phase shift and the magnitude become:

$$\log\left[\Delta\widetilde{T}(\alpha, Q, L, f, \hat{z})\right] = -\gamma_r\hat{z} + \log[K_1\Delta T_s] \tag{13}$$

$$\hat{\phi}(\alpha, Q, L, f, \hat{z}) = -\gamma_i\hat{z} - \operatorname{arctg}\left[\frac{1 + K_2K_3}{K_2 - K_3}\right] \tag{14}$$

where $K_1 = e^{-2\gamma_r L} - 2e^{-\gamma_r L}\cos(\gamma_i L) + 1$, $K_2 = \frac{e^{-\gamma_r L}\cos(\gamma_i L) - 1}{e^{-\gamma_r L}\sin(\gamma_i L)}$, and $K_3 = \frac{\gamma_i}{\gamma_r}$ for the temperature condition, and:

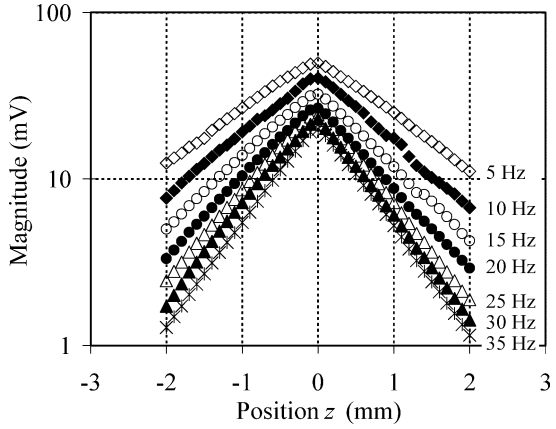


Fig. 4. Magnitude versus position $z$ measured on the P100 carbon fiber at $T_o = 1500$ K, for several frequencies $f$.

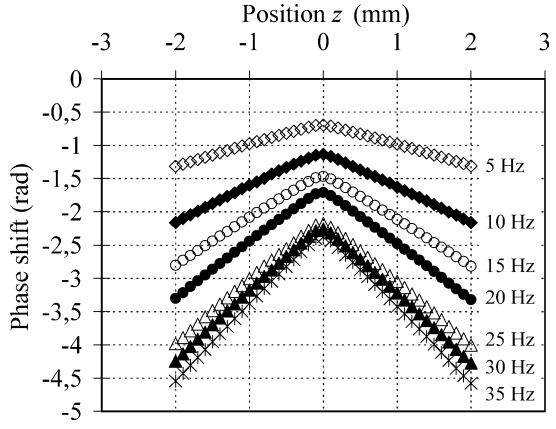


Fig. 5. Phase shift versus position $z$ measured on the P100 carbon fiber at $T_o = 1500$ K, for several frequencies $f$.

$$\log\left[\Delta\widetilde{T}(\alpha, Q, L, f, \hat{z})\right] = -\gamma_r \hat{z} + \log\left[\frac{\Delta\dot{q}_s}{k}\sqrt{\frac{K_1}{(\gamma_r^2+\gamma_i^2)^2 + 4\gamma_r^2\gamma_i^2}}\right] \quad (15)$$

$$\hat{\phi}(\alpha, Q, L, f, \hat{z}) = -\gamma_i \hat{z} - \operatorname{arctg}\left[\frac{1 - K_3^2 + 2K_3K_4}{K_4 - 2K_3 - K_3^2 K_4}\right] \quad (16)$$

where $K_4 = \frac{\cos(\gamma_i L)-1}{\sin(\gamma_i L)}$, for the heat flux condition.

In both temperature or heat flux conditions, the logarithm of the magnitude and the phase shift are linear functions of $\hat{z}$. Measurements realised on a P100 carbon fiber at $T_o = 1500$ K for several frequencies ranging from 5 Hz to 35 Hz are presented in Figs. 4 and 5. The linearity of the magnitude and the phase shift versus $\hat{z}$, far from the laser excitation ($z > a$), is verified. This property will be used for the identification of the thermal diffusivity.

## 5. Identification

For several convenient reasons, some experimental situations are more suitable by the processing of only $\gamma_r$ or $\gamma_i$, whereas for others a combination of $\gamma_r$ and $\gamma_i$ is preferable. Various estimation cases will be examined here in order to choose the best one. For the following calculation, the numerical value of several parameters is fixed in order to determine $Q$ (7): $\varepsilon = 1$, $d = 10$ µm, $\rho = 2260$ kg m$^{-3}$, $c_p = 2000$ J kg$^{-1}$ K$^{-1}$.

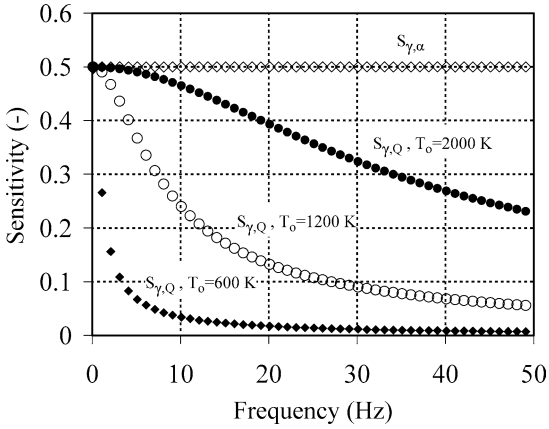


Fig. 6. Sensitivities $S_{\gamma,\alpha}$ and $S_{\gamma,Q}$ for several temperature levels $T_o$.

### 5.1. Estimation from the minimisation on $\gamma_r$ and $\gamma_i$

In both local (9)–(12) or integrated (13)–(16) temperature measurement:

(i) the logarithmic magnitude $\Delta\widetilde{T}$ versus $\hat{z}$ is proportional to $\gamma_r(\alpha, Q, f)$, and
(ii) the phase shift $\hat{\phi}$ versus $\hat{z}$ is proportional to $\gamma_i(\alpha, Q, f)$.

Logically, the estimation of $\alpha$ and $Q$ can be realised from the minimisation of the criterium $J$ which is defined by:

$$J = \sum_{j=1}^{N}\left[\gamma_r^m(f_j) - \gamma_r(\alpha, Q, f_j)\right]^2 \quad (17)$$

using the magnitude measurements or by:

$$J = \sum_{j=1}^{N}\left[\gamma_i^m(f_j) - \gamma_i(\alpha, Q, f_j)\right]^2 \quad (18)$$

using the phase shift measurements, where $\gamma_r^m(f_j)$ and $\gamma_i^m(f_j)$ are the slopes measured at several frequencies $f_j$, while $\gamma_r(\alpha, Q, f_j)$ and $\gamma_i(\alpha, Q, f_j)$ are given by the definitions (7).

The sensitivities absolute values of $\gamma_r$ and $\gamma_i$ on $\alpha$ and $Q$ are identical:

$$S_{\gamma,\alpha} = S_{\gamma_{(r\text{ or }i)},\alpha} = \left|\frac{\alpha}{\gamma_{(r\text{ or }i)}}\frac{\partial\gamma_{(r\text{ or }i)}}{\partial\alpha}\right| = \frac{1}{2}$$
$$S_{\gamma,Q} = S_{\gamma_{(r\text{ or }i)},Q} = \left|\frac{Q}{\gamma_{(r\text{ or }i)}}\frac{\partial\gamma_{(r\text{ or }i)}}{\partial Q}\right| = \frac{Q}{2\sqrt{Q^2+(\pi f)^2}} \quad (19)$$

and are represented in Fig. 6 versus $f$ for three values of $T_o$, $Q$ being a function of $h_o$ (6) which depends on $T_o$ (2). The sensitivity on $\alpha$, not dependent in $T_o$ and $f$, is constant and always greater than the sensitivity on $Q$. When the frequency increases, the influence of the heat losses goes down and the sensitivity on $Q$ decreases. For high temperatures, the heat losses go up and the sensitivity on $Q$ increases. Due to the definition of $\gamma_r$ and $\gamma_i$ (7), the estimation of $\alpha$ and $Q$ following this approach

involves the resolution of a non-linear system using an iterative method. In practical, the convergence of the minimisation is very difficult. For the following, both (magnitude and phase shift) approaches will be called the direct method.

### 5.2. Estimation from the minimisation on $(\pi f)^2$

From the definitions of $\gamma_r$ and $\gamma_i$ (7), $(\pi f)^2$ can be expressed as:

$$F_r(\gamma_r, \alpha^2, \alpha Q) = (\pi f)^2 = \gamma_r^4 \alpha^2 - 2\gamma_r^2 \alpha Q \tag{20}$$

and:

$$F_i(\gamma_i, \alpha^2, \alpha Q) = (\pi f)^2 = \gamma_i^4 \alpha^2 + 2\gamma_i^2 \alpha Q \tag{21}$$

Considering a set of $N$ measurements realised for $f_N$ different frequencies, these relations yield to two $(N \times 2)$ linear over-dimensioning systems:

$$\begin{bmatrix} \gamma_{r,1}^4 & -2\gamma_{r,1}^2 \\ \gamma_{r,2}^4 & -2\gamma_{r,2}^2 \\ \vdots & \vdots \\ \gamma_{r,N}^4 & -2\gamma_{r,N}^2 \end{bmatrix} \begin{bmatrix} \alpha^2 \\ \alpha Q \end{bmatrix} = \begin{bmatrix} (\pi f_1)^2 \\ (\pi f_2)^2 \\ \vdots \\ (\pi f_N)^2 \end{bmatrix} \quad \text{and}$$

$$\begin{bmatrix} \gamma_{i,1}^4 & 2\gamma_{i,1}^2 \\ \gamma_{i,2}^4 & 2\gamma_{i,2}^2 \\ \vdots & \vdots \\ \gamma_{i,N}^4 & 2\gamma_{i,N}^2 \end{bmatrix} \begin{bmatrix} \alpha^2 \\ \alpha Q \end{bmatrix} = \begin{bmatrix} (\pi f_1)^2 \\ (\pi f_2)^2 \\ \vdots \\ (\pi f_N)^2 \end{bmatrix} \tag{22}$$

which solution can be numerically obtained by a direct method [17]. Writing these systems under the matrix notation: $\boldsymbol{X} \cdot \boldsymbol{\beta} = \boldsymbol{Y}$, the solution of Eqs. (22) is given by:

$$\boldsymbol{\beta} = \left(\boldsymbol{X}^{\mathrm{T}} \cdot \boldsymbol{X}\right)^{-1} \cdot \boldsymbol{X}^{\mathrm{T}} \cdot \boldsymbol{Y} \tag{23}$$

which supposes that the estimation of the new parameters $\alpha^2$ and $\alpha Q$ is realised from the minimisation of the criterium $J$ defined by:

$$J = \sum_{j=1}^{N} \left[F_r^m(f_j) - F_r\left(\gamma_r, \alpha^2, \alpha Q\right)\right]^2 \quad \text{and}$$

$$J = \sum_{j=1}^{N} \left[F_i^m(f_j) - F_i\left(\gamma_i, \alpha^2, \alpha Q\right)\right]^2 \tag{24}$$

In these relations, $F_r^m(f_j)$ and $F_i^m(f_j)$ are deduced from the measured frequencies $f_j$, while $F_r(\gamma_r, \alpha^2, \alpha Q)$ and $F_i(\gamma_i, \alpha^2, \alpha Q)$ are calculated by (20) and (21). For the following, the identification using the relation (20) will be called the magnitude method, and the identification using the relation (21) the phase shift method.

The sensitivities absolute values of $F_r$ and $F_i$ on $\alpha^2$ and $\alpha Q$ are similar:

$$S_{F,\alpha^2} = S_{F_{(r \text{ or } i)},\alpha^2} = \left| \frac{\alpha^2}{F_{(r \text{ or } i)}} \frac{\partial F_{(r \text{ or } i)}}{\partial(\alpha^2)} \right| = \frac{\alpha^2 \gamma_{(r \text{ or } i)}^4}{(\pi f)^2}$$

$$S_{F,\alpha Q} = S_{F_{(r \text{ or } i)},\alpha Q} = \left| \frac{\alpha Q}{F_{(r \text{ or } i)}} \frac{\partial F_{(r \text{ or } i)}}{\partial(\alpha Q)} \right| = \frac{2\alpha Q \gamma_{(r \text{ or } i)}^2}{(\pi f)^2} \tag{25}$$

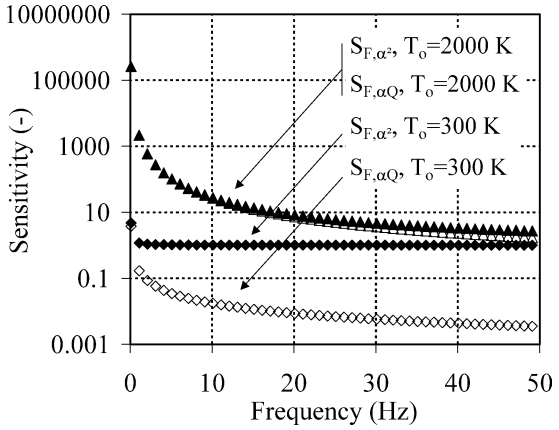


Fig. 7. Magnitude method. Sensitivities $S_{F_r,\alpha^2}$ and $S_{F_r,\alpha Q}$ for $\alpha = 2.212 \times 10^{-8}$ m$^2$ s$^{-1}$ and for two temperature levels $T_o$.

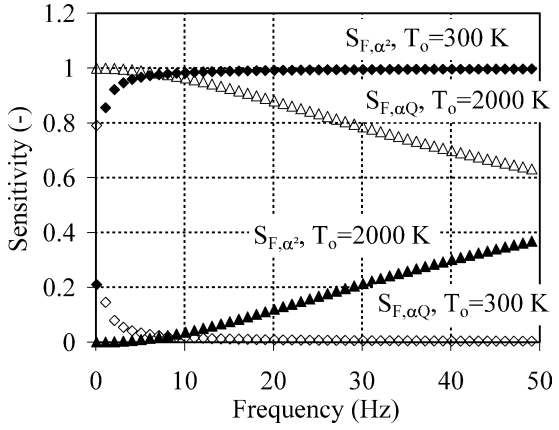


Fig. 8. Phase shift method. Sensitivities $S_{F_i,\alpha^2}$ and $S_{F_i,\alpha Q}$ for $\alpha = 2.212 \times 10^{-8}$ m$^2$ s$^{-1}$ and for two temperature levels $T_o$.

and are respectively represented in Figs. 7 and 8 versus $f$ for two values of $T_o$ (2), (6). For the magnitude method, the sensitivity on both parameters decreases with the frequency. The sensitivity on $\alpha^2$ is always greater than the one on $\alpha Q$, with a wide difference at low temperature but a low gap at very high temperature. As a consequence, the convergence of this method is rapid for the low temperatures but becomes difficult over several hundreds of degrees. For the phase shift method, the sensitivity on $\alpha^2$ is widely greater than the one on $\alpha Q$ at $T_o = 300$ K. At very high temperature, the sensitivity on $\alpha^2$ is lower than the one on $\alpha Q$, the difference decreasing when the frequency goes up. As for the previous, the phase shift method is easy to use for the lower temperatures.

### 5.3. Estimation from the minimisation on the product $\gamma_r \gamma_i$

As it was used for solid bars in the Ångström's method [18], the product $\gamma_r \gamma_i$, calculated from the definitions (7):

$$\gamma_r \gamma_i = \frac{\pi f}{\alpha} \tag{26}$$

can also be employed to estimate the thermal diffusivity. Considering a set of $N$ measurements realised for $f_N$ different

frequencies, this relation yields to a $(N \times 1)$ linear over-dimensioning system:

$$\begin{bmatrix} \pi f_1 \\ \pi f_2 \\ \vdots \\ \pi f_N \end{bmatrix} \frac{1}{\alpha} = \begin{bmatrix} \gamma_{r,1}\gamma_{i,1} \\ \gamma_{r,2}\gamma_{i,2} \\ \vdots \\ \gamma_{r,N}\gamma_{i,N} \end{bmatrix} \tag{27}$$

which solution can be numerically obtained by a direct method [17]. Writing this system under the matrix notation: $\boldsymbol{X} \cdot \boldsymbol{\beta} = \boldsymbol{Y}$ where $\boldsymbol{\beta} = 1/\alpha$, the solution of Eq. (27) is given by the relation (23) which supposes that the estimation of $1/\alpha$ is realised from the minimisation of the criterium $J$ defined by:

$$J = \sum_{j=1}^{N} \left[ \gamma_r^m(f_j)\gamma_i^m(f_j) - \frac{\pi f_j}{\alpha} \right]^2 \tag{28}$$

For the following, the identification using the relation (26) will be called the product method.

The sensitivity absolute value of $\gamma_r\gamma_i$ on $\alpha$ is calculated analytically:

$$S_{\gamma_r\gamma_i,\alpha} = \left| \frac{\alpha}{\gamma_r\gamma_i} \frac{\partial(\gamma_r\gamma_i)}{\partial\alpha} \right| = 1 \tag{29}$$

This value is always greater than the sensitivity computed for the direct (Fig. 6) and the phase (Fig. 8) method. It is lower than the sensitivity computed for the magnitude method (Fig. 7) but keeps constant over the frequency range.

## 6. Comparison between the proposed methods

The direct method (Section 5.1) is very sensitive to the initial values of the estimated parameters $\alpha$ and $Q$. As a consequence, its convergence is generally difficult because the thermal diffusivity of the sample is badly known. So, this method is thrown back.

In order to test the three other methods, a set of 100 pseudo-experimental slopes, resulting from the superposition of noise (standard deviation $\pm 0.04$) on theoretical values $\gamma_i$ and $\gamma_r$ (7), have been computed-generated for $1 < f < 50$ Hz and for drastic estimation conditions: $\alpha = 2 \times 10^{-8}$ m$^2$ s$^{-1}$, $Q = 80$ s$^{-1}$ calculated from: $d = 10$ µm, $\varepsilon = 1$, $k = 0.1$ W m$^{-1}$ K$^{-1}$ (very low thermal conductivity for a fiber), $\rho = 2260$ kg m$^{-3}$, $c_p = 2000$ J kg$^{-1}$ K$^{-1}$, $T = 2000$ K.

### 6.1. Influence of noisy slopes measurements

Measurements are made on a P100 carbon fiber at $T_o = 1500$ K for several frequencies ranging from 5 to 40 Hz fiber. For each frequency $f_j$, the slopes $\gamma_r^m(f_j)$ and $\gamma_i^m(f_j)$ are determined on the sides (right and left) of the excitation. The relative difference $\varepsilon$ between these two values is then calculated as:

$$\varepsilon_{(r\text{ or }i)}(f_j) = 2\frac{\gamma^{m,r}_{(r\text{ or }i)}(f_j) - \gamma^{m,l}_{(r\text{ or }i)}(f_j)}{\gamma^{m,r}_{(r\text{ or }i)}(f_j) + \gamma^{m,l}_{(r\text{ or }i)}(f_j)} \tag{30}$$

The results obtained show that $\varepsilon$ is included in the range $[-1.5\%; 1.5\%]$. In practical, all the experimental cases tested (carbon or ceramic fibers from 1000 to 2500 K) yield a relative difference between both slopes in the range $[-4\%; 4\%]$, for magnitude and phase shift.

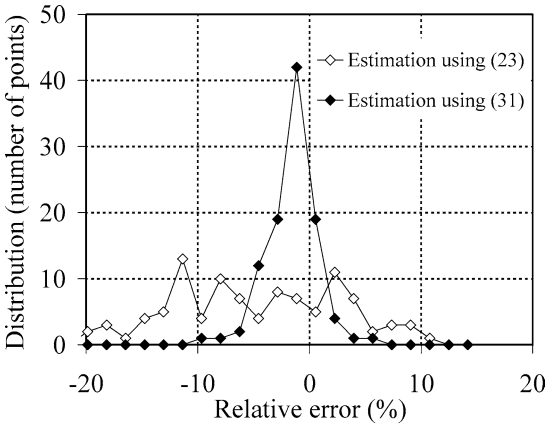


Fig. 9. Interest of the covariance method.

Moreover, the standard deviation $\sigma$ is calculated from each right and left sides records measured on phase shift and magnitude. The least square method is used to fit the records by linear approximation. In practical, $\sigma$ is a function of the frequency for three main reasons. When the frequency increases: (i) the magnitude decreases, (ii) the phase shift increases, whereas (iii) the absolute uncertainty of the lock-in amplifier is constant. Then, the estimation must take into account the standard deviation evaluated for each frequency [17] replacing the relations (23) by:

$$\boldsymbol{\beta} = \left(\boldsymbol{X}^{\mathrm{T}} \cdot \boldsymbol{cov}^{-1} \cdot \boldsymbol{X}\right)^{-1} \cdot \boldsymbol{X}^{\mathrm{T}} \cdot \boldsymbol{cov}^{-1} \cdot \boldsymbol{Y} \tag{31}$$

where the diagonal covariance matrix is given by:

$$\boldsymbol{cov} = \begin{bmatrix} \sigma(f_1)^2 & & & 0 \\ & \sigma(f_2)^2 & & \\ & & \ddots & \\ 0 & & & \sigma(f_N)^2 \end{bmatrix} \tag{32}$$

The relative error on the thermal diffusivity identified following the phase shift method and using or not the covariance formulation is reported in Fig. 9. Taking into account the standard deviation of the slopes leads to reduce this relative error on the thermal diffusivity identified.

### 6.2. Influence of the estimation method

The relative error on the heat losses parameter $Q$ identified following the magnitude and the phase shift methods and using the covariance formulation (31) is presented in Fig. 10. The estimation is biased: the parameter $Q$ is under-estimated in both cases for this example. In addition, a large standard deviation (greater for the phase shift method) is obtained: for the magnitude method, $Q$ is identified with an uncertainty of $\pm\sigma$ and with $\pm 1.5\sigma$ for the phase shift model. The relevant parameter being the thermal diffusivity, the bad estimation of $Q$ is an indirect error source: for these two methods if $Q$ is badly identified, the estimation of $\alpha$ will equally be worse if the sensitivities on both parameters are comparable.

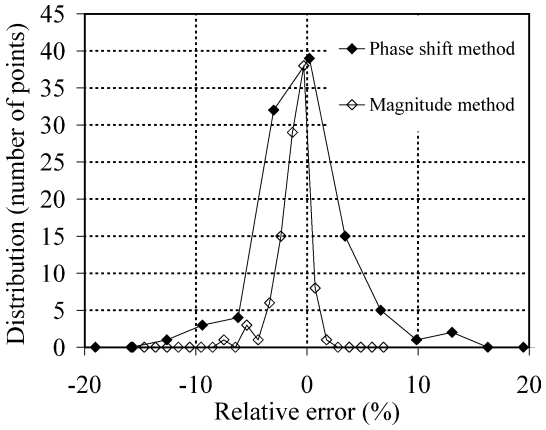


Fig. 10. Comparison between the three methods proposed: relative error on the heat losses parameter $Q$ identified.

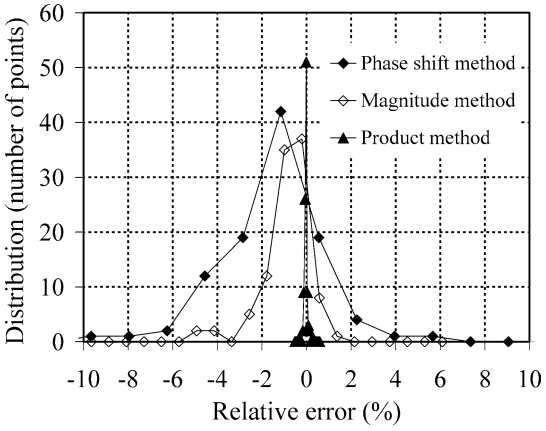


Fig. 11. Comparison between the three methods proposed: relative error on the thermal diffusivity $\alpha$ identified.

The relative error on the thermal diffusivity identified following the three different methods and using the covariance formulation (31) is presented in Fig. 11. The magnitude and the phase shift method always introduce a bias in the estimation: as previously, the thermal diffusivity is under-estimated in both cases. In addition, a large standard deviation always penalises the results: $\alpha$ is identified with an uncertainty of $\pm\sigma/2$ for the magnitude model and with $\pm 3\sigma$ for the phase shift model. On the opposite, the product method gives a distribution centred (no bias) on a null relative error, with a very small standard deviation: $\alpha$ is identified with an uncertainty of $\pm\sigma/80$. This last method is the best to identify the thermal diffusivity. Developed for single fiber, this approach is also applicable for single wire with bigger diameter, making the assumption of thermally thin medium (1D thermal field along the sample).

## 7. Validation

The first measurements have been realised on the Nextel 720 alumina fiber (low conductive material, diameter ≈11 μm), the estimation using the three different methods. The specific heat of the sample is determined on the same apparatus using an original method presented elsewhere [19]. The results, reported on Fig. 12, clearly show the influence of the estimation

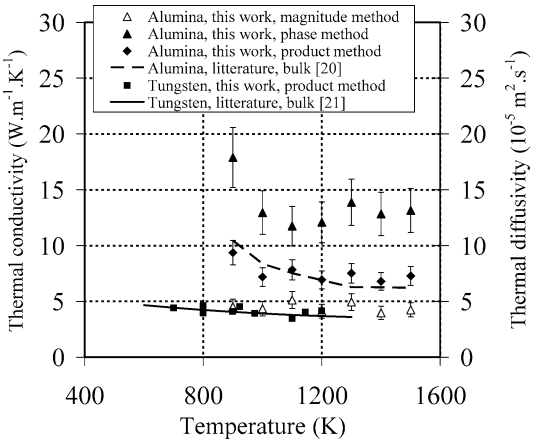


Fig. 12. Thermal conductivity of the Nextel 720 alumina fiber and thermal diffusivity of the tungsten fiber.

method: only the values obtained with the product method are in agreement with Kingery et al. [20]. The second measurements have been made on a tungsten fiber (high conductive material, diameter ≈18 μm), the estimation using the product method. The results, presented on Fig. 12, are in agreement with Touloukian [21]. These experiments on both low and high conductive materials allow the validation of the method and the apparatus, over a wide range of thermal properties.

## 8. Conclusion

An apparatus and an identification method have been developed for the measurement of the thermal diffusivity of single fiber at very high temperature. A 1D direct model, established in the case of temperature or heat flux imposed at the end of the wire, has shown that the logarithmic magnitude and the phase shift of the signal is a linear function of the position along the sample. This property has been verified experimentally on a carbon fiber at 1500 K. Based on this observation, three kinds of estimation have been proposed. A numerical study using noisy simulated measurements, allows to test these methods in order to determine the best one. Finally, for a standard deviation of $\sigma = \pm 4\%$ on the magnitude and phase shift measurements, the identification made with the chosen method leads to a $\pm\sigma/80 = \pm 0.05\%$ uncertainty on the identified diffusivity. Finally, measurements on low and high conductive materials validate the apparatus and the estimation method over a wide range of thermal properties.

## Acknowledgements

The CNRS, Snecma, the CEA and the Region Aquitaine have supported this work.

## References

[1] R. Naslain, Ceramic matrix composites, in: Proceedings of Meeting on High-Temperature Structural Materials, London, 1994.
[2] R. Naslain, Advanced Inorganic Fibers, Kluwer Academic, Boston, 2000.

[3] L. Piraux, B. Nysten, A. Haquenne, J.P. Issi, The temperature variation of the thermal conductivity of benzene-derived carbon fibers, Solid State Commun. 50 (8) (1984) 697–700.
[4] J.P. Issi, B. Nysten, Thermal conductivity of carbon fibers: experimental techniques and structural studies, in: Proceedings of International Symposium on Carbon, I, 1990, pp. 510–513.
[5] X. Zhang, S. Fujiwara, M. Fujii, Short-hot-wire method for the measurement of the thermal conductivity of a fine fiber, High Temperatures—High Pressures 32 (2000) 493–500.
[6] S. Kawabata, Measurement of anisotropic mechanical property and thermal conductivity of single fiber for several high performance fibers, in: Proceedings of the 4th Japan–US Conference on Composite Materials, Washington, Technomic Publishing, Lancaster, 1988, pp. 253–262.
[7] T. Yamane, S. Katayama, M. Todoki, I. Hatta, Thermal diffusivity measurement of single fibers by an AC calorimetric method, J. Appl. Phys. 80 (8) (1996) 4358–4365.
[8] I. Hatta, H. Yao, R. Kato, A. Maesono, Thermal diffusivity measurement of thin films by means of an ac calorimetric method, Rev. Sci. Instruments 56 (1996) 1643–1647.
[9] J.H. Barkoumb, D.J. Land, Thermal diffusivity measurements of thin wires and fibers using a dual-laser photothermal technique, in: Proceedings of the 22nd Thermal Conductivity Conference, 1994, pp. 646–654.
[10] A. Sanchez-Lavega, A. Salazar, Thermal diffusivity measurements in opaque solids by the mirage technique in the temperature range 300 to 1000 K, J. Appl. Phys. 76 (3) (1994) 1462–1468.
[11] J. Jumel, F. Lepoutre, J.P. Roger, G. Neuer, M. Cataldi, F. Enguehard, Microscopic thermal characterization of composites, Rev. Sci. Instruments 74 (1) (2003) 537–539.
[12] H. Le Houdec, D. Rochais, F. Enguehard, J. Jumel, F. Lepoutre, Microscopic thermal characterization at temperatures up to 1000 °C by photoreflectance microscopy, Superlattices and Microstructures 35 (3–6) (2004) 401–408.
[13] M. Oksanen, R. Scholz, Simple Thermal Wave Method for the Determination of the Longitudinal Thermal Diffusivity of SiC-Based Fiber, Review of Progress in Quantitative Nondestructive Evaluation, vol. 17, Plenum, New York, 1998.
[14] J.F. Bisson, D. Fournier, Application of infrared microscopy to thermal diffusivity measurement in refractories at various temperature? High Temperatures—High Pressures 30 (1998) 205–210.
[15] S. Dilhaire, Développement d'un interféromètre très haute résolution pour la caractérisation de composants microélectroniques, PhD thesis, University Bordeaux 1, n°1103, 1994.
[16] J.M. Goyhénèche, M. Laurent, J.F. Sacadura, M. Ferri, C. Fort, Thermal diffusivity measurements of opaque materials at very high temperature by a modulated technique, High Temperature—High Pressures 1 (1999) 525–534.
[17] J.V. Beck, K.J. Arnold, Parameter Estimation in Engineering and Science, John Wiley & Sons, New York, 1997.
[18] H.S. Carslaw, J.C. Jaeger, Conduction of Heat in Solids, University Press, Oxford, 1980.
[19] C. Pradère, J.M. Goyhénèche, J.C. Batsale, S. Dilhaire, R. Pailler, Specific heat measurement of single metallic, carbon and ceramic fibers at very high temperature, Rev. Sci. Instruments 76 (6) (2005) 64901-1-6.
[20] W.D. Kingery, H.K. Bowen, D.R. Uhlmann, Introduction to Ceramics, John Wiley & Sons, New York, 1977.
[21] Y.S. Touloukian, Thermophysical Properties of High Temperature Solid Materials, MacMillan, London, 1967.